HHS Public Access

Author manuscript

Environ Toxicol Pharmacol. Author manuscript; available in PMC 2021 January 01.

Published in final edited form as:

Environ Toxicol Pharmacol. 2020 January ; 73: 103281. doi:10.1016/j.etap.2019.103281.

MICROCYSTIN EXPOSURE WORSENS NONALCOHOLIC FATTY LIVER DISEASE ASSOCIATED ECTOPIC GLOMERULAR TOXICITY VIA NOX-2-MIR21 AXIS

Sutapa Sarkar[1,2,**], **Firas Alhasson**[1,**], **Diana Kimono**[1,2], **Muayad Albadrani**[1,2], **Ratanesh K. Seth**[1,2], **Shuo Xiao**[2], **Dwayne E. Porter**[2], **Geoff I. Scott**[2], **Bryan Brooks**[3], **Mitzi Nagarkatti**[4], **Prakash Nagarkatti**[4], **Saurabh Chatterjee**[1,2,*]

[1]Environmental Health and Disease Laboratory, Department of Environmental Health Sciences, University of South Carolina

[2]NIEHS Center for Oceans and Human Health on Climate Change Interactions, Department of Environmental Health Sciences, University of South Carolina

[3]Department of Environmental Science, Baylor University

[4]Pathology, Microbiology and Immunology, University of South Carolina School of Medicine

Abstract

NAFLD often results in cardiovascular, intestinal and renal complications. Previous reports from our laboratory highlighted NAFLD induced ectopic inflammatory manifestations in the kidney that gave rise to glomerular inflammation. Extending our studies, we hypothesized that existing inflammatory conditions in NAFLD could make the kidneys more susceptible to environmental toxicity. Our results showed that exposure of Microcystin-LR (MC) in NAFLD mice caused a marked increase in cellular scarring with a concomitant increase in mesangial cell activation as observed by increased α-SMA in the extracellular matrix surrounding the glomeruli. Renal tissue surrounding the glomeruli also showed increased NOX2 activation as shown by greater co-localization of p47 Phox and its membrane component gp91Phox both in the mesangial cell and surrounding tissue. Mechanistically, mesangial cells incubated with apocynin, nitrone spin trap DMPO and miR21 inhibitor showed significantly decreased α-SMA, miR21 levels and proinflammatory cytokine release in the supernatant. In parallel, mice lacking miR21, known to be activated by NOX2, when exposed to MC in NAFLD showed decreased mesangial cell activation. Strikingly, phenyl boronic acid incubated cells that were exposed to MC showed significantly

[*]**Author for correspondence:** Dr. Saurabh Chatterjee, Ph.D. Environmental Health and Disease Laboratory, NIEHS Center for Oceans and Human Health on Climate Change Interactions, Department of Environmental Health Sciences, University of South Carolina, Columbia 29208 USA. schatt@mailbox.sc.edu; Tel: 803-777-8120; Fax: 803-777-3391.

[**]Sutapa Sarkar and Firas Alhasson equally contributed to the study.

Contributions

S.C. and F.A. designed experiments. S.S., M.A, R.S., D.K., conducted experiments, interpreted data; S.C., B.B., G.S., D.P., M.N. and P.N., interpreted data, edited manuscript; F.A, S.S. wrote manuscript and analyzed data.

Competing Interests

The authors declare no competing interests.

decreased mesangial cell activation showing that peroxynitrite might be the major reactive species involved in mediation of the activation process, release of proinflammatory micro RNAs and cytokines that are crucial for renal toxicity. Thus, in conclusion, MC exposure causes NOX2 activation that leads to mesangial cell activation and toxicity via release of peroxynitrite that also represses PTEN by the upregulation of miR21 thus amplifying the toxicity.

Keywords

Leptin; NOX-2; NADPH; Mesangial Cells; miR21; Oxidative stress; NAFLD; JAK/STAT

INTRODUCTION

Cyanobacteria are prokaryotic organisms found in fresh and brackish water throughout the world. They mostly grow under specific climatic conditions using key nutrients like nitrogen and phosphorus resulting in cyanobacteria blooms (Bellem et al., 2013). Each type of cyanobacteria produces a specific toxin that is released to the environment after their death (Zhang et al., 2010). Among all cyanotoxins, microcystin is widely dispersed throughout the aquatic world. The microcystin family has almost 90 isoforms, consisting of heptapeptide (β-amino acid(ADDA), alanine (D-ala), D- β -methyl-isoaspartate(D-β-Me-isoAsp), and glutamic acid (D-glu) (Liu and Sun, 2015). Microcystin-LR is one of the most potent toxins released from cyanobacteria and can cause different pathological conditions (Luukkainen et al., 1994). Chronic low dosage of microcystin-LR exposure through different routes, like contaminated drinking water, direct skin contact, or by inhalation, can cause human health problems (Botha et al., 2004). Although the liver is a primary target for microcystin, different organs can be impacted such as the kidneys and the gut (Botha et al., 2004, Humpage et al., 2000). Therefore, microcystin exposure links with various diseases like hepatic inflammation, gastroenteritis, liver and colon cancers (Herfindal and Selheim, 2006, Humpage et al., 2000, Ueno et al., 1996). Inhibition of serine/threonine protein phosphatases, especially protein phosphatase 1 (PP1) and protein phosphatase 2A (PP2A), is the most common pathway of microcystin activity inside cells (Ohta et al., 1992, Svircev et al., 2009, Falconer and Yeung, 1992). Nong *et al* (2007) found that microcystin-LR exposure led to the generation of reactive oxygen species (ROS) through the cytochrome isoform CYP2E1. Furthermore, lipid peroxidation, oxidative stress, and mitochondrial dysfunction can be mediated by microcystin-LR exposure (Nong et al., 2007).

Obesity is one of the most significant public health problems in the world, particularly in developed countries because of its sheer prevalence. The consequences of obesity include premature death, disabilities, and these contribute to the high costs of health care (Patel et al., 2014). Obesity has several medical complications, which include cardiac diseases, hypertension, and liver abnormalities such as Nonalcoholic fatty liver disease (NAFLD) (Fabbrini et al., 2010). NAFLD is a wide spectrum phenomenon including a simple form called nonalcoholic fatty liver, which is characterized by extra fat accumulation without cell damage, and a second more progressive form called Nonalcoholic steatohepatitis (NASH), characterized by high level of inflammation and cell abnormalities (Brunt et al., 2015, Ogden et al., 2007). Oxidative stress-cytochrome P450 pathway plays a critical role in the

advancement of NAFLD to NASH through mediation of lipid peroxidation and NADPH oxidase activation, which in turn leads to the release of proinflammatory cytokines which causes hepatic and extrahepatic cell damage (Seth et al., 2013). Our lab has previously demonstrated that progression of NASH can cause ectopic glomerulonephritis via mesangial cell activation (Alhasson et al., 2016). In-Vitro mesangial cell activation has shown high expression of alpha smooth muscle actin (α SMA) and transforming growth factor-β (TGF-β) after being treated with 4HNE, a marker of lipid peroxidation, while mesangial cell proliferation was attenuated via cytochrome P450 inhibition by using diallyl sulphide (DAS) (Alhasson et al., 2016).

NADPH oxidase is a primary source of reactive oxygen series (ROS) generation. NADPH oxidase 2 (NOX2) has been shown to be highly expressed in different types of cells including mesangial cells, smooth muscle cells, in addition to macrophages (You et al., 2013). NOX2 expression causes several renal diseases and dysfunctions, like ischemia-reperfusion injury (IRI) and diabetic nephropathy (You et al., 2013, Karim et al., 2015). MicroRNAs (miRNAs) are small noncoded mRNAs that play a significant role in regulating gene expression during post-transcription. Among all miRNAs, mir21 takes part in nephritis and renal fibrosis (Bellem et al., 2013). In the kidney, TGF β– SMAD2/3 signaling pathway upregulates miR21, that can inhibit SMAD7 and PTEN causing further activation of TGF β downstream signaling (Zhang et al., 2010). The present study examined the hypothesis that microcystin exposure increases NAFLD severity causing renal damage and glomerulonephritis through mesangial cell activation. Exposure to the toxin microcystin possibly led to the activation of NOX2 and generation of reactive oxygen species, specifically peroxynitrite. Increased peroxynitrite expression was observed by depicting 3-nitrotyrosine immunoreactivity in NAFLD mice exposed to microcystin, which lead to the activation of TGF β signaling pathway. Increased miR21 expression and subsequent decreased PTEN expression was observed in the mice treated with microcystin, suggesting that upregulated miR21 may lead to the inhibition of PTEN, that resulted in the development of a fibrotic phenotype in the murine kidneys Also, increased α-SMA immunoreactivity depicted mesangial cell activation in the microcystin treated mice, along with the release of pro-inflammatory cytokines. The mesangial cell activation and increased oxidative stress caused due to activation of NOX2, were greatly attenuated in the NOX2 knockout mice (P47 Phox KO) treated with microcystin, which suggested an association of NOX2 with oxidative stress and fibrogenesis activity (Djamali et al., 2012, Djamali et al., 2009). Also, a significant decrease in TGF β expression and a significant increase in PTEN expression was observed in the miR21 knockout mice compared to the wild type mice. Therefore, mechanistically, our results from in vivo and in vitro models showed that microcystin exposure could be linked with NOX2 mediated miR21 upregulation, resulting in the release of fibrogenesis markers and proinflammatory cytokines thus inducing heightened nephrotoxicity.

MATERIAL AND METHODS

The chemicals used for the experiments were purchased from Sigma Aldrich and were of analytical grade. Microcystin-LR toxin was purchased from Cayman Chemicals (Ann Arbor, MI) and leptin was purchased from BioVision (Milpitas, CA). Anti-3 nitrotyrosine (3NT),

anti-TGF-β, anti- GP91 phox, anti-P47phox, and anti-alpha smooth muscle actin primary antibodies were purchased from Abcam (Cambridge, MA). Anti-β-actin and anti-PTEN antibodies were purchased from Santa-Cruz Biotechnology. Biotinylated secondary antibodies (species specific) were purchased from Vector Laboratories (Vectastain Elite ABC kit, Burlingame, CA). The Streptavidin-horseradish peroxidase was also bought from Vector Laboratories. ProLong Diamond antifade mounting media with DAPI and species specific Alexa fluor (fluorescence conjugated) secondary antibodies were purchased from Thermo Fisher Scientific (Waltham, MA). The IHC-Tek was purchased from IHCWORLD (Catalog# IW-1000). Mice models (wild type and gene specific knockout (KO) mice) were purchased from the Jackson Laboratories (Bar Harbor, ME). The mice were fed with special diet which was purchased from Research Diets (New Brunswick, NJ) to develop the diseased model. Once the mice were sacrificed, the mice kidney tissue was paraffinized on slides by the Instumentation Resource Facility (IRF)in University of South Carolina School of Medicine and AML Laboratories (Baltimore, MD).

Animal Model

Pathogen-free, male, C57BL/6J wild type (WT), p47phox gene deleted mice (p47 phoxKO, B6(cg)-Ncf1M1J/J(JAC004742) and micro RNA 21 gene deleted mice (miR21 KO, B6.129S6-Mir21tm1 Yoli/J) were fed with methionine choline deficient high-fat-diet (MCD-HFD, 60% kCal) from 8 weeks to 14weeks to induce Non-alcoholic fatty liver disease (NAFLD). Another group of mice were fed with normal chow diet which was used as the control group for the study. All mice had ad libitum access to food and water and were housed in a temperature-controlled room at 23–24°C with a 12-hour light/dark cycle. After completion of the doses, the mice were euthanized and they weighed about 25 grams at the time of euthanization. All animals were treated in strict accordance with the NIH Guide for the Humane Care and Use of Laboratory Animals and local IACUC standards. The institutional review board at the University of South Carolina approved the experiments that were performed for this study.

Exposure to environmental toxin Microcystin

The chow diet fed wild-type mice, MCD-HFD fed wild type mice and the MCD-HFD fed gene specific knockout mice(P47phox KO, miR21 KO), at 8 weeks were administered with microcystin (10μg/ kg of mice body weight). The dosage was given for 5 days in a week maintaining the 24 hour interval for two weeks, through the intraperitoneal route, to assess the choric exposure effects of microcystin. The mice were then euthanized at completion of the treatment and the blood serum and kidney tissue was collected for further processing.

Experimental Models Used

The experimental groups used for this study were the wild type mice fed with chow diet only (Lean Control) and exposed to microcystin (LC+MC), wild type mice fed with methionine choline deficient-high fat diet only (NAFLD), wild type mice fed with methionine choline deficient-high fat diet and then exposed to microcystin (NAFLD + MC), one group of p47 phox KO mice fed with methionine choline deficient-high fat diet and exposed with microcystin (p47phox KO+MC) and another group of miRNA 21 KO mice fed with methionine choline deficient- high fat diet and then exposed to microcystin (miRNA 21 KO

+MC). A number of 6 mice per group were allocated to their respective cages according to the procedure of randomization. A total of 30 mice were used in the experiments for the study.

Cell culture

Kidney Mesangial cell line (CRL-1927) was purchased from ATCC (Manassas, VA) and maintained in Dulbelcco's modified eagle's medium (DMEM), Corning (Tewksbury, MA). To this DMEM media, 100U/ml Penicillin and 100ug/ml streptomycin from Gibco (Grand Island, NY) were added. The media was then supplemented with 10% fetal bovine serum, Atlanta biologicals (Norcross, GA), 2mM glutamine at 37°C in a humidified atmosphere of 5% CO2. The cells were serum starved (DMEM with 0.25% FBS) overnight before starting the treatment. A set of cells were treated with leptin 100ng/ml, another group were treated with MC-LR (20μM) separately or combination with leptin. Another group of cells were incubated with Apocynin (100 μM) (inhibitor of NADPH oxidase activity), Phenyl Boronic Acid (FBA) (100 μM) (a Peroxynitrite scavenger), 100 mM of the spin trap 3-[[2-(Biotinamido)ethyl] dithio] propionic Acid 4'-(Hydroxymethyl) (DMPO) and the miR21 inhibitor, followed by the treatment of the leptin and microcystin in these groups. The cells were treated for 24 hours and then they were harvested in Trizol reagent (Invitrogen, Grand 82 Island, NY) for mRNA extraction and RIPA Lysis Buffer for the protein extraction. Few cells were seeded on 18mm coverslips from MatTek Corp, (Ashland, MA), which were then used for the immunofluorescence staining procedure after the treatment was completed. Also, the cell supernatants were collected and stored in −80°C for future use.

Hematoxylin and eosin staining (H&E)

Formalin-fixed kidney tissues were paraffin embedded by the IRF facility in the USC School of medicine. Experiments were then performed on the kidney tissue sectionsstained with hematoxylin and eosin by the IRF facility, following the manufacturer's protocol.

Immunohistochemistry

The kidneys were collected from each animal and fixed in 10% neutral buffered formalin (Sigma Aldrich, Missouri, USA). These formalin-fixed, paraffin embedded tissues were cut in 5μm thick sections by the IRF facility in the USC School of Medicine. The sections were deparaffinized using the standard protocol of incubating with xylene twice for 3 min, then with xylene: ethanol (1:1) for 3 min, which was further rehydrated through a series of ethanol dilutions (twice with 100%, 95%, 70%, 50%), followed by twice with distilled water, and finally rinsed twice with PBS (Sigma-Aldrich). The epitope retrieval solution and steamer from IHC-World, Woodstock, MD was used for the epitope retrieval of the deparaffinized sections for 45 minutes. The slides were washed once with IX PBST (1X Phosphate Buffered Saline with 0.2% Tween 20) and then were blocked with 3% H202 for 15 minutes, which blocks the endogenous peroxidases. It was then finally blocked with the IHC-TEK solution for 1 hour, washed twice with 1X PBST and was incubated overnight with the primary antibody for TGF-β (1:300) (Abcam, Cambridge, MA) at 4 degrees. Following the manufacturer's protocols the species specific biotinylated conjugated secondary antibody (1:150) was added and the streptavidin conjugated with HRP were used to perform antigen-specific immunohistochemistry. 3, 3' Diaminobenzidine (Sigma-Aldrich,

St.Louis, MO) was used as a chromogenic substrate and Mayer's hematoxylin counterstain were used for the tissue sectiobs. After the final washes with 1X PBST, the kidney sections were mounted in Simpo mount (GBI Laboratories, Mukilteo, WA) and were observed under 20x and 40x objectives using an Olympus BX51microscope (Olympus, America). Morphometric analysis was done using CellSens Software from Olympus America (Center Valley, PA).

Immunofluorescence

IN VIVO, formalin-fixed, paraffin-embedded tissue sections were subjected to deparaffinization according to the above mentioned standard protocol. After epitope retrieval of the deparaffinized sections with the epitope retrieval solution and steamer (IHC World), the kidney sections were blocked with 3% Bovine Serum Albumin (Sigma Aldrich) in IX PBST for 1 hour, followed by blocking for another 1 hour with IHC TEK (purchased from IHC WORLD). The sections were washed thrice with the 1X PBST for 10 minutes each and then incubated with the primary antibodies anti α-SMA (1:300), anti-GP91phox (1:300), anti-p47phox (1:300), and anti-3NT (1:300). The sections were incubated overnight at 4 degrees and washed thoroughly before the addition of the secondary antibodies to remove any non-specific binding. Species-specific fluorescence conjugated anti-IgG secondary antibodies were used at the dilution of 1:150. The sections were mounted in a ProLong Diamond antifade reagent with DAPI (Life Technologies, Carlsbad, CA). Images were taken under ×20 and ×60 oil objectives with an Olympus BX51 microscope. IN VITRO, on completion of the treatments, the cells attached on the cover slips were fixed with pre-warmed 10% neutral buffered saline for 15 minutes in room temperature. The cells were then permeabilized with PBS containing 0.1% Triton X (Sigma), and were blocked with 3% BSA, 0.2% Tween (Fisher), 10% FBS in PBS. The cells were incubated with primary antibodies anti- α-SMA (1:300), anti-3NT (1:250), washed thrice thoroughly and followed by incubation with species-specific Alexa Fluor 633 and 488 secondary antibodies (1:150 dilution). The stained cells attached on the coverslips were mounted on slides with ProLong Diamondantifade reagent with DAPI (Life Technologies) and viewed under ×40 objectives with an Olympus BX51 microscope.

Quantitative Real-Time Polymerase Chain Reaction

Gene expression levels in kidney tissue samples were measured by the two-step qRT-PCR protocol. The kidney tissue was homogenized and centrifuged to remove any extra tissue particles or debris. Total RNA was then isolated from the homogenized kidney tissue in TRIzol reagent (Invitrogen)according to the manufacturer's instructions and purified with the use of RNAse mini kit columns (Qiagen, Valencia, CA). Purified RNA (1000ng) was converted to cDNA using the iScript cDNA synthesis kit (Bio-Rad) following the manufacturer's standard protocol. qRT-PCR was performed with the gene-specific primers using SsoAdvanced SYBR Green supermix (Bio-Rad) and CFX96 thermal cycler (Bio-Rad). Threshold Cycle (Ct) values for the selected genes were normalized against 18S (internal control) values in the same sample. The relative fold change was calculated by the $2^{-\Delta\Delta Ct}$ method. The sequences for the mouse specific primers used for real time PCR are provided in (table 1). Total miRNA was isolated from cells grown in a monolayer by homogenization in Qiazol reagent (Qiagen) following the manufacturer's instructions. The purification was

done by using miRNAse mini kit columns (Qiagen). Purified miRNA (1,000 ng) was converted to cDNA using miScript cDNA synthesis kit (Qiagen) following the manufacturer's protocol. qRT-PCR was performed with miRNA-specific primers (Qiagen) using miScript SYBR Green PCR master mix (Qiagen) and CFX96 thermal cycler (Bio-Rad). Ct values for the selected gene were normalized against RNU6–2 (internal miR expression control) values in the same sample.

Western blot

SDS PAGE-Resolved protein bands were transferred to nitrocellulose membrane using precut nitrocellulose/filter paper sandwiches (Bio-Rad Laboratories, Hercules, CA) and Trans-Blot Turbo transfer system (Bio-Rad) in case of low molecular weight proteins and using wet transfer module from Invitrogen for high molecular weight proteins. The membrane was incubated with the primary antibody for PTEN and β-actin (Santa Cruz Biotech.) at dilutions (1:1000), which was then incubated with species-specific horseradish peroxidase-conjugated secondary antibodies (1:5000 dilution) for 1.5 hours. Pierce ECL Western Blotting substrate (Thermo Fisher Scientific, Rockford, IL) was used for detection of the protein bands. The blot was imaged using G:BoxChemi XX6 (Syngene imaging systems) and subjected to densitometry analysis using Image J.

TUNEL assay

Mesangial cells adhered on coverslips were used for a TUNEL assay using an Apoptag Fluorescein in Situ Apoptosis Detection Kit (Millipore, Temecula, CA) following the manufacturer's protocol. The cells were counterstained with propidium iodide in antifade reagent (Millipore). Stained sections were imaged at magnification of ×40 using the Olympus BX51 microscope.

Statistical analysis

All *in vivo* experiments were repeated three times with at least five mice per group (N=5; data from each group of mice were pooled). The statistical analysis was carried out by unpaired t-test and analysis of variance (ANOVA) for assessing difference between multiple groups. For all analysis $P<0.05$ was considered statistically significant. For experiments involving 3 or more groups, data were evaluated using one-way ANOVA with multiple comparison Bonferroni post hoc analysis. Data are expressed as mean ± SEM, or as absolute number or percentage for categorical variables. The significance level was set at $\alpha = 5\%$ for all comparisons.

RESULTS

Microcystin-LR exposure causes glomerular immune cellular infiltrations and glomerular damage in underlying NAFLD

Sub-chronic dose of microcystin-LR can cause glomerular damages and infiltration of immune cells especially eosinophils (Milutinovic et al., 2003). To study whether an underlying NAFLD condition induces heightened nephrotoxicity due to microcystin exposure, renal tissue sections were visualized following Hematoxylin and Eosin (H&E) staining. Our results showed thickness in the glomerular wall in mice group fed with

methionine and choline deficient high fat (MCD-HFD) diet exposed to microcystin-LR compared to mice fed with MCD-HFD diet without microcystin treatment and normal chow diet mice exposing to microcystin-LR (Fig1). In addition, infiltration of immune cells and proliferation of mesangial cells were observed to be high in NAFLD group exposed to microcystin. Microcystin-LR exposure showed significant increase of mesangial cell proliferation in NAFLD mice, as assessed by significant increase in alpha smooth muscle actin (α-SMA) expression. The increased immunoreactivity of α-SMA, which is a specific mesangial cell activation marker, was significantly increased in NAFLD mice treated with microcystin compared to NAFLD mice and lean mice exposed to microcystin (*$P < 0.05$; Fig2, A and B) suggesting that microcystin exposure in NAFLD results in worsening of diseased pathology in the kidney.

Microcystin potentiates NAFLD induced renal inflammation and secretion of pro inflammatory cytokines in renal tissue

We have shown previously that environmental toxin like bromodichloromethane(BDCM), which is metabolized by cytochrome P 450 (CyP2E1), is augmented in NAFLD mice to release significant high level of cytokines in renal tissue (Alhasson et al., 2016). To study the effect of microcystin-LR administration in mice, genetic expression of proinflammatory cytokines were analyzed by qRT-PCR. Results showed that mRNA expression of pro-inflammatory IL-1β was significantly higher in NALFD mice treated with microcystin-LR and lean mice exposed to microcystin compared to NAFLD mice alone (Fig3, A, *P<0.05). Similar results were obtained for mRNA expression of MCP-1, CD68, F4/80 where NAFLD mice treated with microcystin and lean mice exposed to microcystin had significant increase in expression compared to the NAFLD mice (Fig3; B, C, and D *P< 0.05) respectively. This result showed that microcystin exposure may potentiate the release of pro-inflammatory cytokines in kidney, which in turn may lead to renal inflammation and renal tissue damage.

Microcystin exposure activates mesangial cell NOX2 and mediates mesangial cell NOX2 generated peroxynitrite

NOX2 upregulation causes oxidative stress resulting in renal hypertrophy, dysregulation in renal function, inflammation, and fibrosis (Li et al., 2017). To prove the role of microcystin in induction of NADPH 2 oxidase (NOX2) in progressive NAFLD, we studied the membrane association of two subunits (P47phox and GP91phox) of NOX2 by using immunofluorescence microscopy in mice tissue samples. Results were analyzed for the number of colocalization/overlay events (shown by yellow). Results showed that the NAFLD mice exposed to microcystin-LR group had a significant increase in the NOX2 colocalization events compared with the NAFLD only group (#P < 0.01) (Fig.4 A and B). Lean mice group treated with microcystin-LR showed less colocalization events when compared to the NAFLD mice treated with microcystin-LR (#P < 0.01) (Fig.4 A and B). Furthermore, no significant change in colocalization events was observed between lean mice exposed to microcystin and NAFLD only group. The above outcomes showed that microcystin induced p47phox expression in NAFLD and assisted in the membrane association of p47phox and gp91phox that might cause oxidative stress in the mesangial cells and surrounding tissues. To demonstrate that mesangial cell NOX2 activation resulted in peroxynitrite generation and played a role in mesangial cell activation, experiments were

performed in the NAFLD mice model. Results showed that NAFLD mice fed with microcystin had significant increase in mesangial cell proliferation compared with NAFLD only group, as assessed by alpha smooth muscle actin reactivity (α-SMA) (#P < 0.01) (Fig.5 A and B). P47phox KO mice had significant decrease in α-SMA activity compared to the NAFLD mice exposed to microcystin (#P < 0.01) (Fig.5 A and B). Our results also showed that 3-nitrotyrosine immunoreactivity was significantly increased in the NAFLD+MC group compared to the NAFLD group (*P < 0.05) (Fig. 5, C and D). P47phox KO mice had significant decrease in 3-nitrotyrosine immunoreactivity activity compared with NAFLD +MC (*P < 0.05) (Fig. 5, C and D). The results suggested that microcystin is significantly associated with an increase in 3-nitrotyrosine immunoreactivity, and peroxynitrite might be a key molecular regulator in causing oxidative stress and mesangial cell activation.

Microcystin administration upregulates miR21 expression in mesangial cells

Among all miRNAs that have been identified, miR21 has been upregulated in different kidney diseases, such as chronic kidney disease and acute kidney disease. Although miR21 expression existed in health kidney condition, high level of miR21 expression was identified in kidney diseases, particularly in fibrosis (Gomez et al., 2015). Experiments were performed with mesangial cells to prove that microcystin, through its activation of NOX2 increased miR21 expression (Fig. 6). Results showed that mesangial cells treated with 10 μM microcystin-LR and 100ng leptin (MC+Leptin) had 2.5-fold increase in miR21 expression compared to mesangial cell control (*P<0.05). Leptin treated mesangial cells were plated to represent a NAFLD microenvironment and were exposed to NOX2 inhibitor apocynin (MC+Leptin+Apo) or peroxynitrite scavenger Phenyl Boronic Acid (MC+Leptin +FBA). The groups MC+Leptin+Apo and MC+Leptin+FBA had significant decrease in miR21 expression compared with MC+Leptin group (*P< 0.05). To prove that microcystin activates mesangial cell in vivo through high expression of miR21, we performed experiments with NAFLD mice kidney tissues. Results showed that NAFLD+MC group had a significant increase in α-SMA expression, as shown in immunofluorescence microscopy (2.7-fold increase) compared to NAFLD only group (Fig.7 A and C) (*P< 0.05). miR21 KO mice treated with microcystin (miR21 KO + MC) had a significant decrease in α-SMA expression compared to NAFLD+MC mice group (*P< 0.05).

Next, we explored the role of microcystin mediated miR21 upregulation in mesangial cells by determining immunoreactivity of α-SMA in mesangial cells. The results showed that mesangial cells treated with leptin and microcystin (leptin+MC) had a significant increase in α-SMA compared to mesangial cell control (Fig. 7. B and D) (*P< 0.05). Furthermore, mesangial cells incubated with leptin and microcystin and treated with Apocynin (leptin +MC+Apo), FBA (leptin+MC+FBA), or miR21 inhibitor (leptin+MC+mir21 inh.) had a significant decrease in α-SMA immunoreactivity compared to leptin+MC group (Fig. 7. C and D) (*P< 0.05). The above results showed that mesangial cell activation is dependent on miR21 upregulation. Inhibition of miR21 attenuates mesangial cell activation and reduces pro-inflammatory cytokines release.

Peroxynitrite- miR21 axis drives mesangial cell activation and death

Recent study from our laboratory has shown that NADPH oxidase activation leads to peroxynitrite generation and result in a cascade of events, such as NF-κB activation (McCullough, 2006). To support that NOX2 mediates peroxynitrite generation resulting in mesangial cell activation and to find the link between peroxynitrite generation and miR21, experiments were performed in a mesangial cell line. Results showed that mesangial cells treated with leptin and microcystin (leptin+MC) had a significant increase in 3-nitro tyrosine (3NT) (almost 1.8-fold increase) compared to control group. (Fig. 8. A and C) (*$P < 0.05$). Mesangial cells that were treated with leptin and microcystin and were subsequently incubated with Apocynin (Leptin+MC+Apo), FBA (Leptin+MC+FBA), or miR21 inhibitor (Leptin+MC+miR21 inh.) had a significant decrease in peroxynitrite formation compared with Leptin+MC mesangial cell group, as assessed by 3NT immunoreactivity (*$P < 0.05$).

While ROS activation and peroxynitrite generation are consequences of microcystin-LR exposure, apoptosis can be another outcome of MC-LR exposure in renal kidney cell line (Alverca et al., 2009). One possible mechanistic pathway can be through endoplasmic reticular damage(Qi et al., 2016). To observe whether microcystin exposure caused cell death, experiments were performed in mesangial cell line with or without leptin and/or microcystin. Results showed that leptin+MC group had a significant increase in number of apoptotic cells (1.5- fold increased) compared with mesnagial cells only or mesangial cells +leptin that served as subsequent control. (Fig. 8. B and D) (*$P < 0.05$). Leptin+MC+Apo, Leptin+MC+FBA, and Leptin+MC+miR21 inh (an antagomir generated by in situ transfection) had a significant decrease in apoptotic cell number compared with leptin+MC group (Fig. 8. C and D) (*$P < 0.05$). The results above suggested that microcystin-LR augmented NAFLD renal immunotoxicity through peroxynitrite – miR21 axis, as assessed in the 3NT immunoreactivity, which was subsequently blocked by miR21 inhibitor. Therefore, it was depicted that microcystin-LR led to cell death in mesangial cells in presence of NAFLD, as observed by the TUNEL staining.

Microcystin-LR mediated NOX2 activation and corresponding induction of miR21 in NAFLD are crucial for TGF-β signaling pathway

Our laboratory has previously shown that NADPH oxidase activation and subsequent upregulation of miR21 are required for TGF-β signaling pathway which in turn leads to fibrogensis (Dattaroy et al., 2015). To support the hypothesis that microcystin via NOX2-mir21 axis causes upregulation of TGF-β signaling pathway, experiments were performed in NAFLD mice model. Results showed that kidney tissue slices from NAFLD+MC group had a significant increase in TGF-β immunoreactivity (as showed in immunohistochemistry) compared with NAFLD only group (Fig. 9. A and B) (*$P < 0.05$)(shown by brown staining). On the other hand, miR21 KO mice (miR21KO + MC) had a significant decrease in TGF-β compared to the NAFLD+MC group. The morphometry analysis showed that miR21 KO+ MC had a two-fold decrease in TGF-β immunoreactivity compared with NAFLD+MC, while no difference in TGF-β reactivity was found between miR21 KO+MC group and NAFLD only group. (Fig9. A and B).

Post transcription of miR21 downregulates tumor suppressor PTEN in vivo

Repression of PETN and SMAD-7 play a key role in the TGF-β signaling pathway. To prove that NOX2-miR21 axis represses PTEN expression level which is a target protein for miR21 and a mechanistic switch for TGF-beta signaling, we performed experiments in the NAFLD mice model. Results showed that microcystin administration decreased levels of PTEN in the NAFLD+MC group, as shown by Western blot analysis compared to the NAFLD only (Fig. 10. A and B). The results also showed a subsequent increase in the levels of PTEN in P47phox KO +MC and miR21 KO +MC mice. The results therefore suggested that activation of NOX2 and subsequent upregulation of miR21 might lead to the inhibition of PTEN which in turn activates the TGF-β downstream signaling pathway leading to the fibrotic pathology in the kidney.

DISCUSSION

The present study reports a redox-mediated process and its subsequent effect on the micro RNA as a possible toxicological mechanism in the NAFLD kidney following chronic exposure of microcystin-LR, a cyanobacterial heptapeptide toxin. The resultant effect heightens ectopic inflammation in the kidney in NAFLD. Microcystin enhances nonalcoholic fatty liver disease (NAFLD) leading to renal immunotoxicity via mesangial cell activation, as indicated by an increase α-SMA immunoreactivity (Floege et al., 1992). We also showed that mesangial cell proliferation mediated by NOX2 activation and peroxynitrite generation led to miR21 overexpression. Furthermore, using the rodent model of NAFLD, we observed that miR21 activation caused the onset of TGF-β downstream pathway by the repression of PTEN, thereby causing renal inflammation.

There is increasing evidence that a condition of NAFLD, which has high risks of progressing to NASH, cirrhosis, and hepatocellular carcinoma, can have comorbidities that may include kidney diseases and cardiovascular complications. The multiple hit theory is the most likely explanation for the progression of NAFLD to NASH. Oxidative stress, inflammatory adipokines, and environmental toxins are second hits to the progression of the NAFLD condition and its comorbidities(Alhasson et al., 2016). In addition, microcystin plays a critical role in ROS generation in the animal models and in the different cell lines (Wei et al., 2008). In the present study, we used microcystin-LR as an environmental toxin and which acted as a causative factor that led to the activation of NOX2 in renal tissues of NAFLD mice. Interestingly, our results showed that microcystin-LR altered the glomerular morphology by increasing wall thickness and increased immune cell filtration as indicated in the histopathology sections of the kidney. The alteration of glomerular structure led to mesangial cell activation and proliferation, as assessed by α-SMA immunoreactivity. Consequently, a significant increase in the levels of proinflammatory cytokines, like IL1β, MCP-1, F4/80, and CD68 has been shown (Fig.3). Mesangial cell proliferation is always associated with lipid peroxidation which triggers NOX2 upregulation and peroxynitrite generation (Alhasson et al., 2016, Fan et al., 2007). Mesangial cell activation and NOX2 activation, as indicated by NOX2 subunit colocalization, is significantly decreased in P47phox KO mice. Peroxynitrite formation also decreases in P47phox KO mice, as assessed

by 3-nitro tyrosine, a marker of peroxynitrite-mediated nitrosative stress, indicating that mesangial cell activation is depended on the NOX2 pathway and peroxynitrite generation.

MicroRNAs (miRNAs) are small noncoding RNAs that reduce gene expression post-transcriptionally, thereby modulating the activity of signaling pathways, including stress responses in many physiologic and pathologic processes. Among all miRNAs, miR21 mediates damage to the kidney via reduction of several molecular targets (Chau et al., 2012). We found a high level of miR21 expression level in the mesangial cell exposed to microcystin-LR. We also found α-SMA, a proliferative marker of mesangial cells to be repressed after the cell was incubated with miR21 inhibitor. Mesangial cell proliferation was also downregulated in miR21 KO mice treated with microcystin-LR. These results support the conclusion that miR21 plays a prominent role in microcystin induced mesangial cell activation. Microcystin-LR exposure triggered cell death (apoptosis) as a biochemical feature of microcystin toxicity. Several studies have also shown that microcystin damages mitochondria via variant mechanisms that alters mitochondrial features resulting in ROS formation and pro-apoptotic cytokine release (Lemasters et al., 1998). In the present study, we identified that mesangial cells suffered from apoptosis after microcystin exposure, and that the apoptotic events were decreased when mesangial cells were incubated with apocynin and FBA. This result indicates that the apoptotic process in microcystin-induced mesangial cell death is NOX2 dependent, as assessed by the reduced number of positive apoptotic cells (Tunel assay) after administration of NADPH oxidase inhibitor and a specific scavenger and blocking agent of peroxynitrite. Activation of the TGF-β pathway, which regulates different cell processes and functions, including cell proliferation and apoptosis, has been demonstrated in several pathological conditions, suc h as chronic kidney disease (Massague and Wotton, 2000). TGF-β mesangial extracellular matrix deposition is the most common component in fibrogenesis. More recently, our studies showed that NADPH oxidase-mediated miR21 activation significantly upregulated TGF-β protein level in the condition of NAFLD (Dattaroy et al., 2015). The results also showed repression of PTEN in the NAFLD +MC group, which target the SMAD2/3 pathway, a critical step in TGF-β signaling activation. The expression was subsequently higher in the miR21KO group suggesting a role of miR21 in inhibiting PTEN. NAFLD mice treated with microcystin-LR showed high immunoreactivity of TGF-β compared with the NAFLD group (Fig.9. A and B) which suggests that chronic exposure to microcystin activates the TGF-β pathway and produces extracellular matrix which is a vital sign preceding fibrosis. On the other hand, miR21 KO mice showed less TGF-β immunoreactivity, which meant the activation of TGF-β pathway was miR21 dependent. Furthermore, PTEN protein levels were attenuated in mice exposed to microcystin, in parallel, mice with specific genes knocked out like P47phox and miR21 had a significant increase in PTEN protein level (fig. 10. A and B). The results above proved the existence of microcystin activated NOX2- miR21 axis, which attenuates PTEN expression resulting in the TGF-β signaling pathway. Taken together, our data describe a novel mechanistic role of microcystin-LR in augmenting NAFLD caused nephrotoxicity via NOX2- miR21 axis in mesangial cells resulting in the release of TGF-β and tubular inflammation. Our results will help advance the current knowledge of the microcystin-LR mechanistic toxicity and conclude that targeting NOX2 by using a specific inhibitor might

be a good therapeutic mechanism and it might be a candidate for an interventional strategy to reduce ectopic inflammatory events in NAFLD with possible microcystin exposure.

Acknowledgements

The authors gratefully acknowledge the technical services of Benny Davidson at the IRF, University of South Carolina School of Medicine and AML Labs (Baltimore MD). We also thank the Instrumentation resource facility (IRF) at the University of South Carolina for equipment usage and consulting services. This work has been supported by NIH Awards 2P20GM103641-06,1P01ES028942-01 and P01AT003961 to Saurabh Chatterjee, 1P01ES028942-01 to Dwayne Porter and Geoff I Scott, P01AT003961, P20GM103641, R01AT006888, R01ES019313, R01MH094755 to Mitzi Nagarkatti and Prakash S. Nagarkatti.

REFERENCES

ALHASSON F, DATTAROY D, DAS S, CHANDRASHEKARAN V, SETH RK, SCHNELLMANN RG & CHATTERJEE S 2016 NKT cell modulates NAFLD potentiation of metabolic oxidative stress-induced mesangial cell activation and proximal tubular toxicity. Am J Physiol Renal Physiol, 310, F85–F101. [PubMed: 26447219]

ALVERCA E, ANDRADE M, DIAS E, SAM BENTO F, BATOREU MC, JORDAN P, SILVA MJ & PEREIRA P 2009 Morphological and ultrastructural effects of microcystin-LR from Microcystis aeruginosa extract on a kidney cell line. Toxicon, 54, 283–94. [PubMed: 19393682]

BELLEM F, NUNES S & MORAIS M 2013 Cyanobacteria toxicity: potential public health impact in South Portugal populations. J Toxicol Environ Health A, 76, 263–71. [PubMed: 23514068]

BOTHA N, VAN DE VENTER M, DOWNING TG, SHEPHARD EG & GEHRINGER MM 2004 The effect of intraperitoneally administered microcystin-LR on the gastrointestinal tract of Balb/c mice. Toxicon, 43, 251–4. [PubMed: 15033322]

BRUNT EM, WONG VW, NOBILI V, DAY CP, SOOKOIAN S, MAHER JJ, BUGIANESI E, SIRLIN CB, NEUSCHWANDER-TETRI BA & RINELLA ME 2015 Nonalcoholic fatty liver disease. Nat Rev Dis Primers, 1, 15080. [PubMed: 27188459]

CHAU BN, XIN C, HARTNER J, REN S, CASTANO AP, LINN G, LI J, TRAN PT, KAIMAL V, HUANG X, CHANG AN, LI S, KALRA A, GRAFALS M, PORTILLA D, MACKENNA DA, ORKIN SH & DUFFIELD JS 2012 MicroRNA-21 promotes fibrosis of the kidney by silencing metabolic pathways. Sci Transl Med, 4, 121ra18.

DATTAROY D, POURHOSEINI S, DAS S, ALHASSON F, SETH RK, NAGARKATTI M, MICHELOTTI GA, DIEHL AM & CHATTERJEE S 2015 Micro-RNA 21 inhibition of SMAD7 enhances fibrogenesis via leptin-mediated NADPH oxidase in experimental and human nonalcoholic steatohepatitis. Am J Physiol Gastrointest Liver Physiol, 308, G298–312. [PubMed: 25501551]

DJAMALI A, REESE S, HAFEZ O, VIDYASAGAR A, JACOBSON L, SWAIN W, KOLEHMAINEN C, HUANG L, WILSON NA & TORREALBA JR 2012 Nox2 is a mediator of chronic CsA nephrotoxicity. Am J Transplant, 12, 1997–2007. [PubMed: 22568654]

DJAMALI A, VIDYASAGAR A, ADULLA M, HULLETT D & REESE S 2009 Nox-2 is a modulator of fibrogenesis in kidney allografts. Am J Transplant, 9, 74–82. [PubMed: 18976289]

FABBRINI E, SULLIVAN S & KLEIN S 2010 Obesity and nonalcoholic fatty liver disease: biochemical, metabolic, and clinical implications. Hepatology, 51, 679–89. [PubMed: 20041406]

FALCONER IR & YEUNG DS 1992 Cytoskeletal changes in hepatocytes induced by Microcystis toxins and their relation to hyperphosphorylation of cell proteins. Chem Biol Interact, 81, 181–96. [PubMed: 1370395]

FAN J, LI Y, LEVY RM, FAN JJ, HACKAM DJ, VODOVOTZ Y, YANG H, TRACEY KJ, BILLIAR TR & WILSON MA 2007 Hemorrhagic shock induces NAD(P)H oxidase activation in neutrophils: role of HMGB1-TLR4 signaling. J Immunol, 178, 6573–80. [PubMed: 17475888]

FLOEGE J, JOHNSON RJ & COUSER WG 1992 Mesangial cells in the pathogenesis of progressive glomerular disease in animal models. Clin Investig, 70, 857–64.

GOMEZ IG, MACKENNA DA, JOHNSON BG, KAIMAL V, ROACH AM, REN S, NAKAGAWA N, XIN C, NEWITT R, PANDYA S, XIA TH, LIU X, BORZA DB, GRAFALS M, SHANKLAND SJ, HIMMELFARB J, PORTILLA D, LIU S, CHAU BN & DUFFIELD JS 2015 Anti-microRNA-21 oligonucleotides prevent Alport nephropathy progression by stimulating metabolic pathways. J Clin Invest, 125, 141–56. [PubMed: 25415439]

HERFINDAL L & SELHEIM F 2006 Microcystin produces disparate effects on liver cells in a dose dependent manner. Mini Rev Med Chem, 6, 279–85. [PubMed: 16515466]

HUMPAGE AR, HARDY SJ, MOORE EJ, FROSCIO SM & FALCONER IR 2000 Microcystins (cyanobacterial toxins) in drinking water enhance the growth of aberrant crypt foci in the mouse colon. J Toxicol Environ Health A, 61, 155–65. [PubMed: 11036504]

KARIM AS, REESE SR, WILSON NA, JACOBSON LM, ZHONG W & DJAMALI A 2015 Nox2 is a mediator of ischemia reperfusion injury. Am J Transplant, 15, 2888–99. [PubMed: 26104383]

LEMASTERS JJ, NIEMINEN AL, QIAN T, TROST LC, ELMORE SP, NISHIMURA Y, CROWE RA, CASCIO WE, BRADHAM CA, BRENNER DA & HERMAN B 1998 The mitochondrial permeability transition in cell death: a common mechanism in necrosis, apoptosis and autophagy. Biochim Biophys Acta, 1366, 177–96. [PubMed: 9714796]

LI MS, ADESINA SE, ELLIS CL, GOOCH JL, HOOVER RS & WILLIAMS CR 2017 NADPH oxidase-2 mediates zinc deficiency-induced oxidative stress and kidney damage. Am J Physiol Cell Physiol, 312, C47–C55. [PubMed: 27806940]

LIU J & SUN Y 2015 The role of PP2A-associated proteins and signal pathways in microcystin-LR toxicity. Toxicol Lett, 236, 1–7. [PubMed: 25922137]

LUUKKAINEN R, NAMIKOSHI M, SIVONEN K, RINEHART KL & NIEMELA SI 1994 Isolation and identification of 12 microcystins from four strains and two bloom samples of Microcystis spp.: structure of a new hepatotoxin. Toxicon, 32, 133–9. [PubMed: 9237346]

MASSAGUE J & WOTTON D 2000 Transcriptional control by the TGF-beta/Smad signaling system. EMBO J, 19, 1745–54. [PubMed: 10775259]

MCCULLOUGH AJ 2006 Pathophysiology of nonalcoholic steatohepatitis. J Clin Gastroenterol, 40 Suppl 1, S17–29.

MILUTINOVIC A, ZIVIN M, ZORC-PLESKOVIC R, SEDMAK B & SUPUT D 2003 Nephrotoxic effects of chronic administration of microcystins -LR and -YR. Toxicon, 42, 281–8. [PubMed: 14559079]

NONG Q, KOMATSU M, IZUMO K, INDO HP, XU B, AOYAMA K, MAJIMA HJ, HORIUCHI M, MORIMOTO K & TAKEUCHI T 2007 Involvement of reactive oxygen species in Microcystin-LR-induced cytogenotoxicity. Free Radic Res, 41, 1326–37. [PubMed: 17963120]

OGDEN CL, YANOVSKI SZ, CARROLL MD & FLEGAL KM 2007 The epidemiology of obesity. Gastroenterology, 132, 2087–102. [PubMed: 17498505]

OHTA T, NISHIWAKI R, YATSUNAMI J, KOMORI A, SUGANUMA M & FUJIKI H 1992 Hyperphosphorylation of cytokeratins 8 and 18 by microcystin-LR, a new liver tumor promoter, in primary cultured rat hepatocytes. Carcinogenesis, 13, 2443–7. [PubMed: 1282096]

PATEL AV, HILDEBRAND JS & GAPSTUR SM 2014 Body mass index and all-cause mortality in a large prospective cohort of white and black U.S. Adults. PLoS One, 9, e109153. [PubMed: 25295620]

QI M, DANG Y, XU Q, YU L, LIU C, YUAN Y & WANG J 2016 Microcystin-LR induced developmental toxicity and apoptosis in zebrafish (Danio rerio) larvae by activation of ER stress response. Chemosphere, 157, 166–73. [PubMed: 27219292]

SETH RK, KUMAR A, DAS S, KADIISKA MB, MICHELOTTI G, DIEHL AM & CHATTERJEE S 2013 Environmental toxin-linked nonalcoholic steatohepatitis and hepatic metabolic reprogramming in obese mice. Toxicol Sci, 134, 291–303. [PubMed: 23640861]

SVIRCEV Z, KRSTIC S, MILADINOV-MIKOV M, BALTIC V & VIDOVIC M 2009 Freshwater cyanobacterial blooms and primary liver cancer epidemiological studies in Serbia. J Environ Sci Health C Environ Carcinog Ecotoxicol Rev, 27, 36–55. [PubMed: 19204863]

UENO Y, NAGATA S, TSUTSUMI T, HASEGAWA A, WATANABE MF, PARK HD, CHEN GC, CHEN G & YU SZ 1996 Detection of microcystins, a blue-green algal hepatotoxin, in drinking

water sampled in Haimen and Fusui, endemic areas of primary liver cancer in China, by highly sensitive immunoassay. Carcinogenesis, 17, 1317–21. [PubMed: 8681449]

WEI Y, WENG D, LI F, ZOU X, YOUNG DO, JI J & SHEN P 2008 Involvement of JNK regulation in oxidative stress-mediated murine liver injury by microcystin-LR. Apoptosis, 13, 1031–42. [PubMed: 18594987]

YOU YH, OKADA S, LY S, JANDELEIT-DAHM K, BARIT D, NAMIKOSHI T & SHARMA K 2013 Role of Nox2 in diabetic kidney disease. Am J Physiol Renal Physiol, 304, F840–8. [PubMed: 23389458]

ZHANG JG, WANG JJ, ZHAO F, LIU Q, JIANG K & YANG GH 2010 MicroRNA-21 (miR-21) represses tumor suppressor PTEN and promotes growth and invasion in non-small cell lung cancer (NSCLC). Clin Chim Acta, 411, 846–52. [PubMed: 20223231]

Highlights

- Microcystin exposure in NAFLD hastens mesangial cell activation
- Mesangial cell proinflammatory events are a fallout of NOX 2 activation following microcystin exposure
- NOX-2 mediated peroxynitrite modulates kidney pathology in microcystin exposure in NAFLD
- Peroxynitrite activates miR21 and subsequently leads to proinflammatory pathology via repression of PTEN

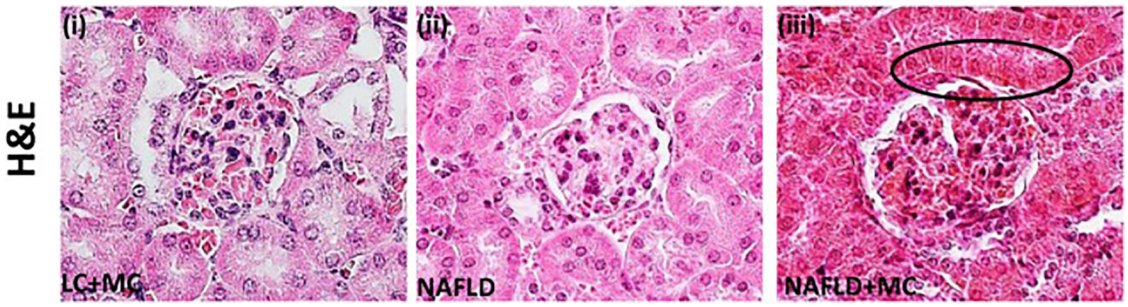

Fig 1: Microcystin increased immune cell filtration in the glomerulus:

Microcystin-LR exposure exacerbated immune cell infiltration in glomeruli anddamaged the glomerular structure. Formalin-fixed, paraffin-embedded 5 μm kidney tissue sections from lean mouse control, wild type mouse control fed with MCD-HFD diet (NAFLD), and another mice group fed with MCD-HFD diet and exposed to microcystin (NAFLD+MC) were used for hematoxylin and eosin staining. **(i-iii):** Hematoxylin and eosin staining was performed in the kidney tissue sections for the groups (Lean+ MC; i), (NAFLD; ii) and (NAFLD+MC; iii). Images were taken at 60X. (*P<0.05).

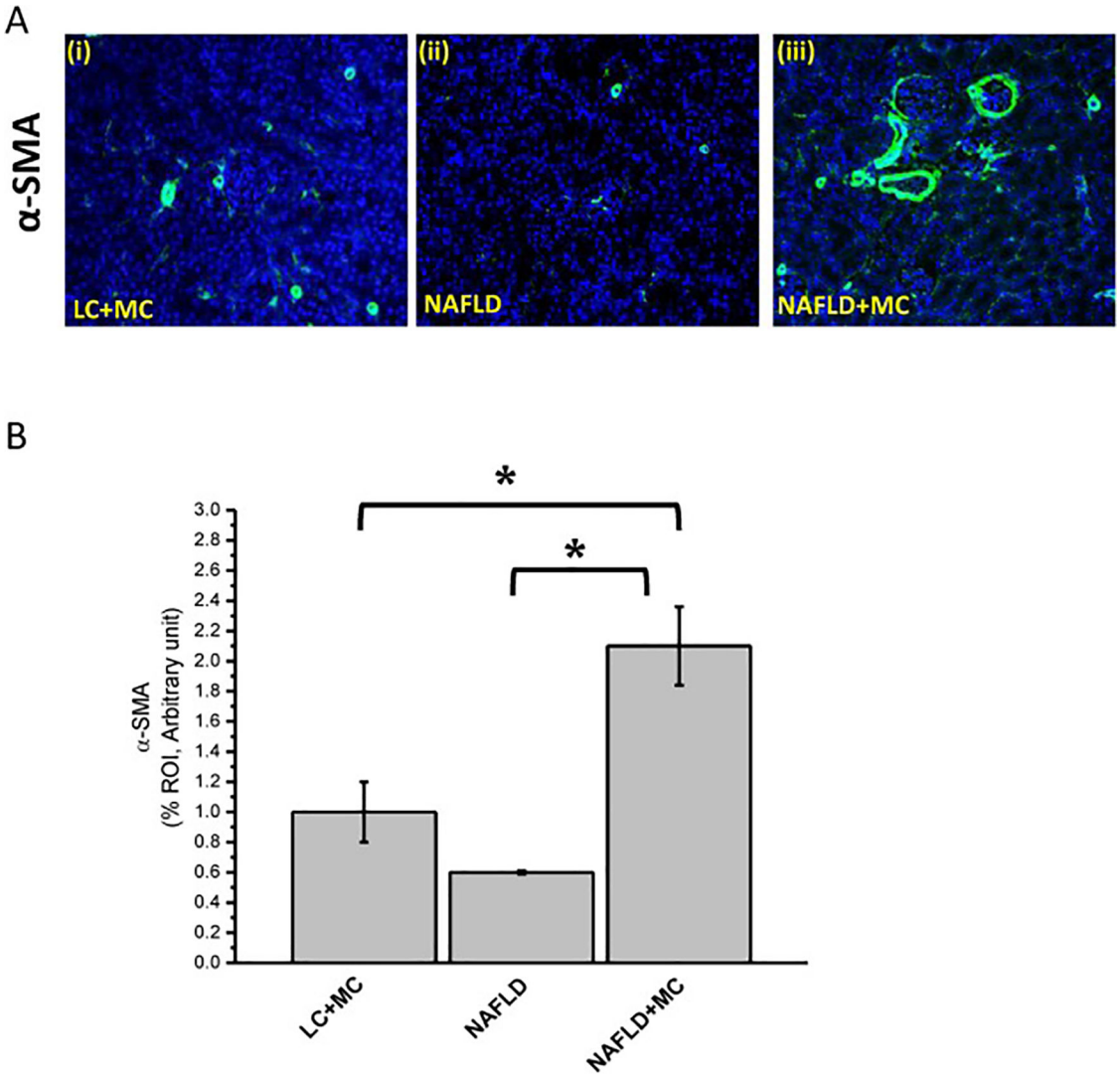

Fig 2: Microcystin exposure augment mesangial cell activation in NAFLD.

Formalin-fixed, paraffin-embedded 5 μm kidney tissue sections from lean mouse control, wild type mouse control fed with MCD-HFD diet (NAFLD), and mice group fed with MCD-HFD diet exposed to microcystin (NAFLD+MC) were used for immunofluorescence imaging. **(A) (i-iii):** Immunoreactivity of alpha smooth muscle actin (α-SMA, a marker for mesangial cell activation) as shown by immunofluorescence in kidney slices from mice groups NAFLD which serve as a control, NAFLD mice exposed NAFLD+MC, lean+ MC. Images were taken at 20X. **(B)** Morphometric analysis of α-SMA immunoreactivity (mean data measured as arbitrary light units from three separate microscopic fields were plotted on y-axis) in NAFLD, NAFLD+MC, and lean+MC groups (*P<0.05). The graph shows a summary of the data, represented as mean SD (n=5 mice per group). Variables were compared for significance using two-way analysis of variance and the Bonferroni test (*, P value between 0.01 and 0.001).

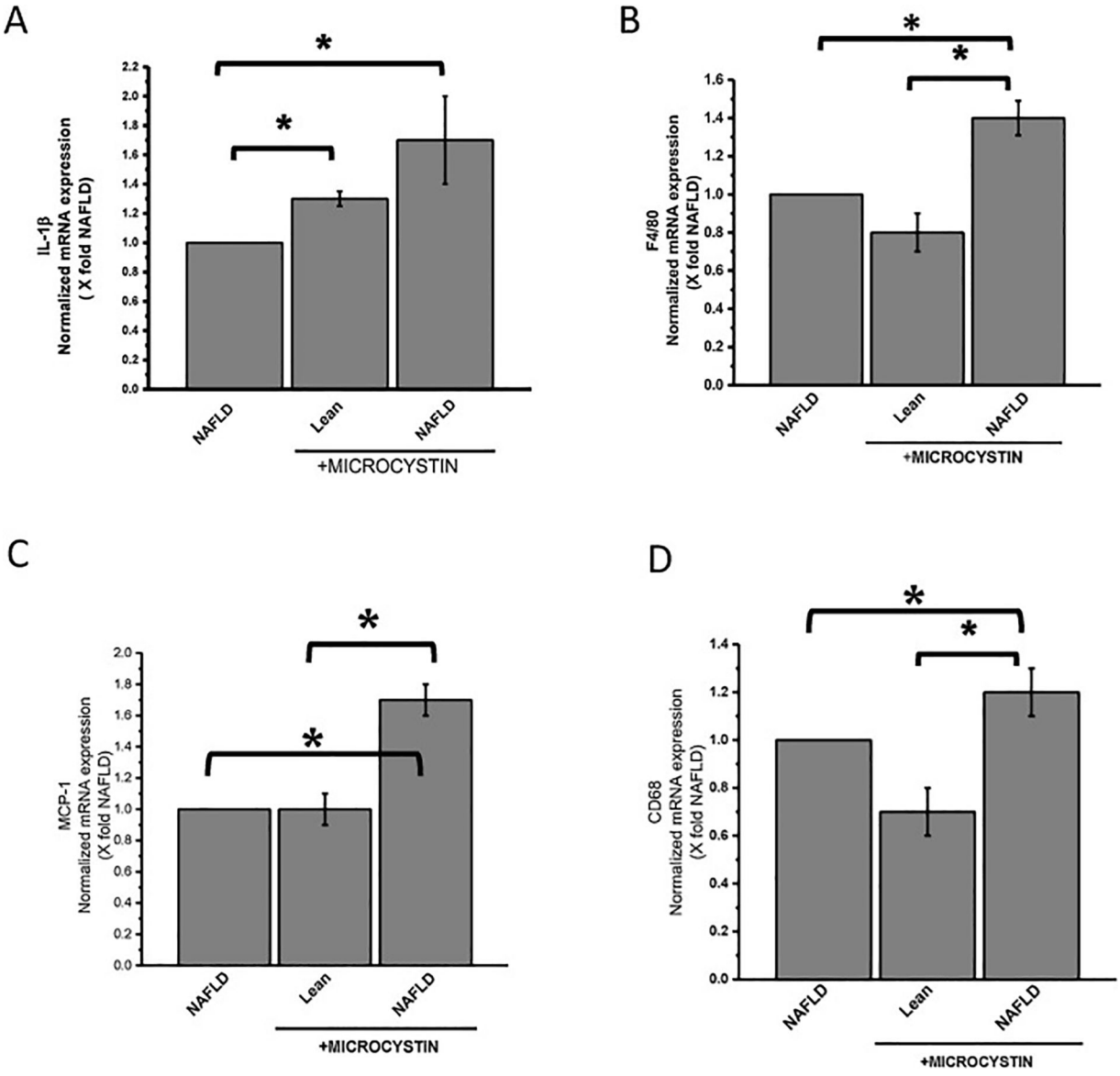

Fig 3: Microcystin exposure heighten glomerular inflammation in NAFLD.

Kidney tissue from lean mouse control, wild type mouse control fed with MCD-HFD diet (NAFLD), and another mice group fed with MCD-HFD diet exposed to microcystin (NAFLD+MC) were used formRNA expression analysis of IL-1β, MCP-1, CD68, and F4/80 genes. **(A)**mRNA expressions of IL-1β. **(B)** mRNA expressions of MCP-1. **(C)**mRNA expressions of CD68. **(D)** mRNA expressions of F4/80. All mRNA expression had been assessed by quantitative real-time PCR (qRTPCR) and expressions were normalized against NAFLD group (*P<0.05). Variables were compared for significance using two-way analysis of variance and the Bonferroni test (*, P value between 0.01 and 0.001).

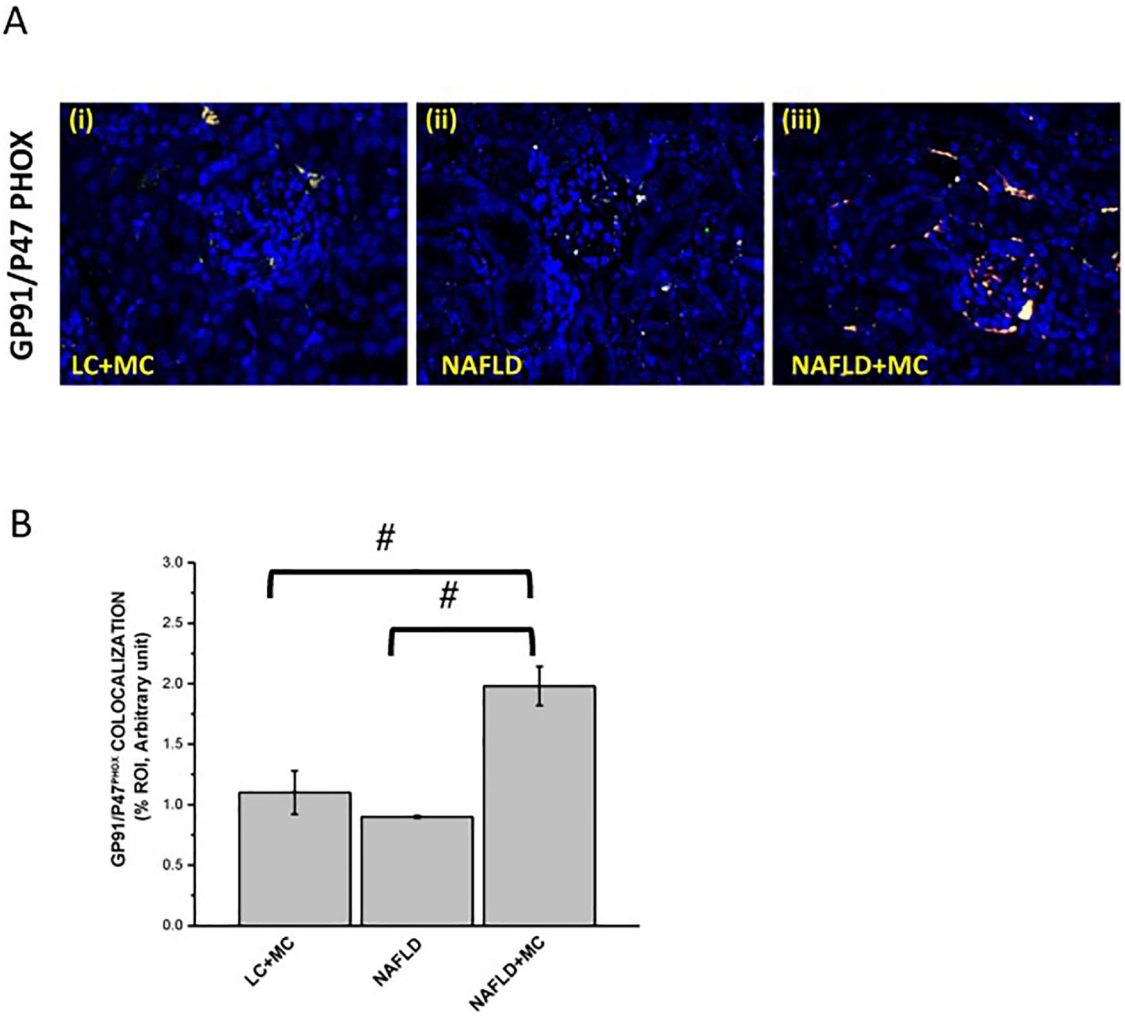

Fig 4: Microcystin exposure activates mesangial cell NADPH oxidase (NOX2) via transport of the cytosolic subunit (P47phox) to the membrane and its colocalization with the membranous subunit (GP91phox).

Formalin-fixed, paraffin-embedded 5 μm kidney tissue sections were used for immunofluorescence imaging. **(A)(i-iii**) Immunofluorescence for P47PhOx (Green and GP-91 Phox (Red) co-localization (Yellow) in kidney slices from mice fed with MCD-HFD diet (NAFLD), NAFLD mice exposed to microcystin-LR (NAFLD+MC), and P47phox gene deficient mice fed with MCD-HFD diet and exposed to microcystin-LR (P47phox KO +MC). **(B)** Morphometric analysis of GP91/P47phox colocalized in NAFLD, NAFLD+MC, P47phox KO+MC group of mice. All immunofluorescent Images were taken at 20X and mean colocalization was measured as arbitrary light units from three separate microscopic fields were plotted on y-axis) (#P<0.05). Variables were compared for significance using two-way analysis of variance and the Bonferroni test (#, P value between 0.01 and 0.05)

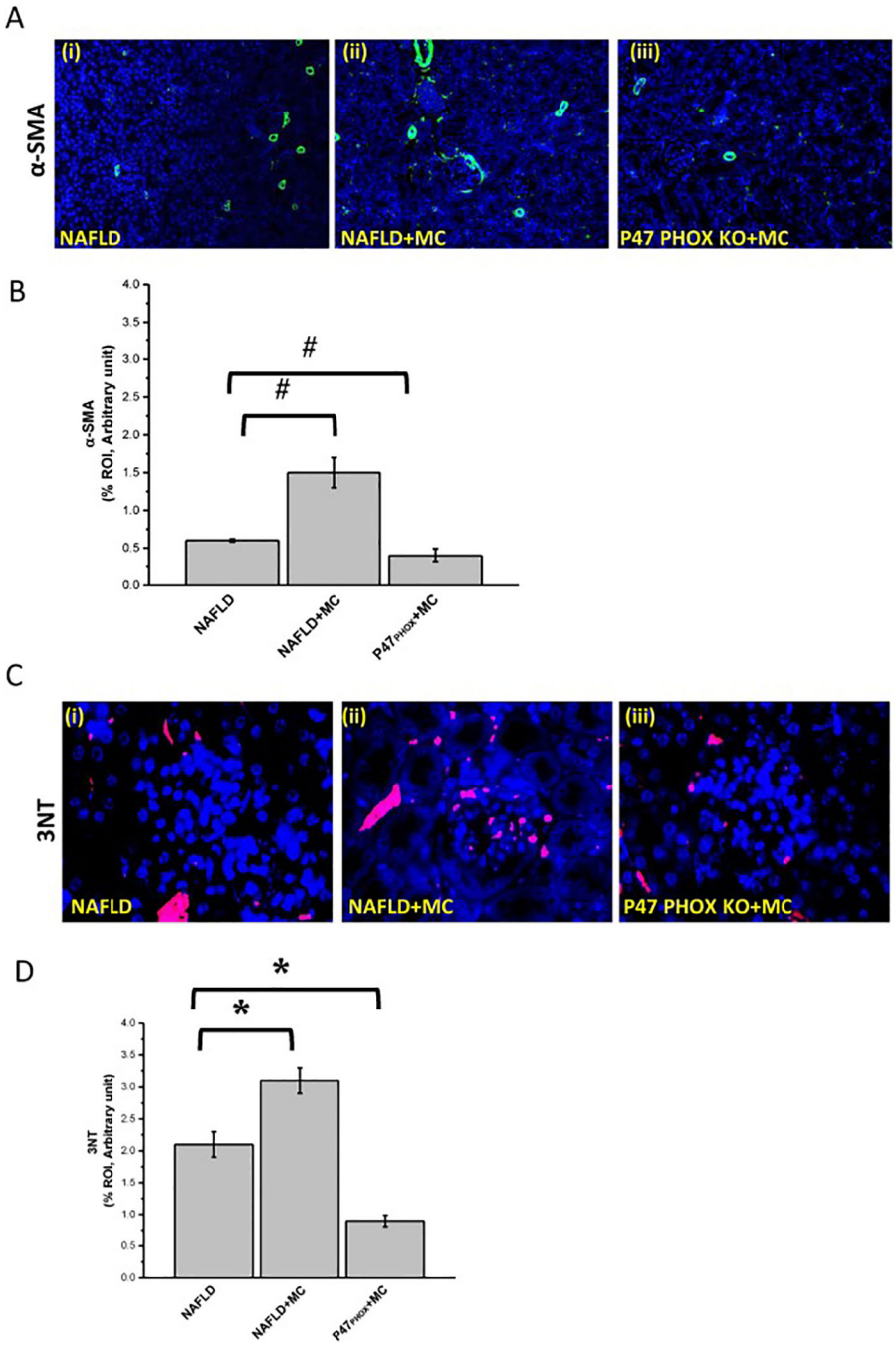

Fig 5. Microcystin-LR generates peroxynitrite via NADPH oxidase (NOX2) activation.

Formalin-fixed, paraffin-embedded 5 μm kidney tissue sections were used for immunofluorescence staining.**(A) (i-iii)** Immunofluorescence for α-SMA (green) immunoreactivity in kidney tissue from mice fed MCD-HFD diet (NAFLD), NAFLD mice exposed to microcystin-LR (NAFLD+MC), and P47phox gene deficient mice fed with MCD-HFD diet and exposed to microcystin-LR (P47phox KO + BDCM) images were taken in 20X. **(B)** Morphometric analysis of α-SMA immunoreactivityin NAFLD, NAFLD+MC, P47phox KO+MC group of mice. All images were taken at 40X and mean colocalization

was measured as arbitrary light units from three separate microscopic fields were plotted on y-axis) (#P<0.05). The graph shows a summary of the data, represented as mean SD (n=5 mice per group). Variables were compared for significance using two-way analysis of variance and the Bonferroni test (#, P value between 0.01 and 0.05) **(C)(i-iii)** Immunofluorescence of 3-Nitro-tyrosine (Red) immunoreactivityin kidney slices from (NAFLD) which served as a control, NAFLD+MC, and P47phox KO+ MC, Images were taken at 60X. **(D)** Morphometric analysis of 3-Nitrotyrosine immunoreactivity (mean data from three separate microscopic fields were plotted on Y-axis) in NAFLD, NAFLD+MC and P47phox KO groups of mice (*P<0.05). Variables were compared for significance using two-way analysis of variance and the Bonferroni test (*, P value between 0.01 and 0.001).

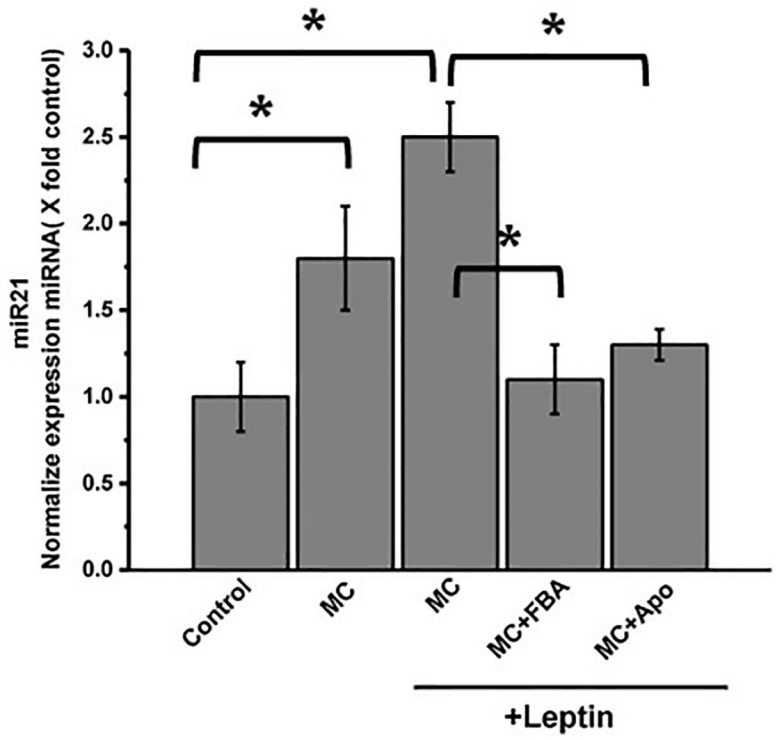

Fig 6: Microcystin-LR-induced NADPH oxidase activation mediates upregulation of micro-RNA 21 (miR21) in the mesangial cells.

qRTPCR analysis of miR21 expression was analyzed in mesangial cells, (control), mesangial cells incubated with leptin and treated with microcystin (MC+MC+leptin), mesangial cells incubated with leptin and treated with both microcystin and apocynin (MC +Apo+leptin), and mesangial cells incubated with leptin and treated with both microcystin and FBA (MC+FBA+leptin). (*P < 0.05). Variables were compared for significance using two-way analysis of variance and the Bonferroni test (*, P value between 0.01 and 0.001)

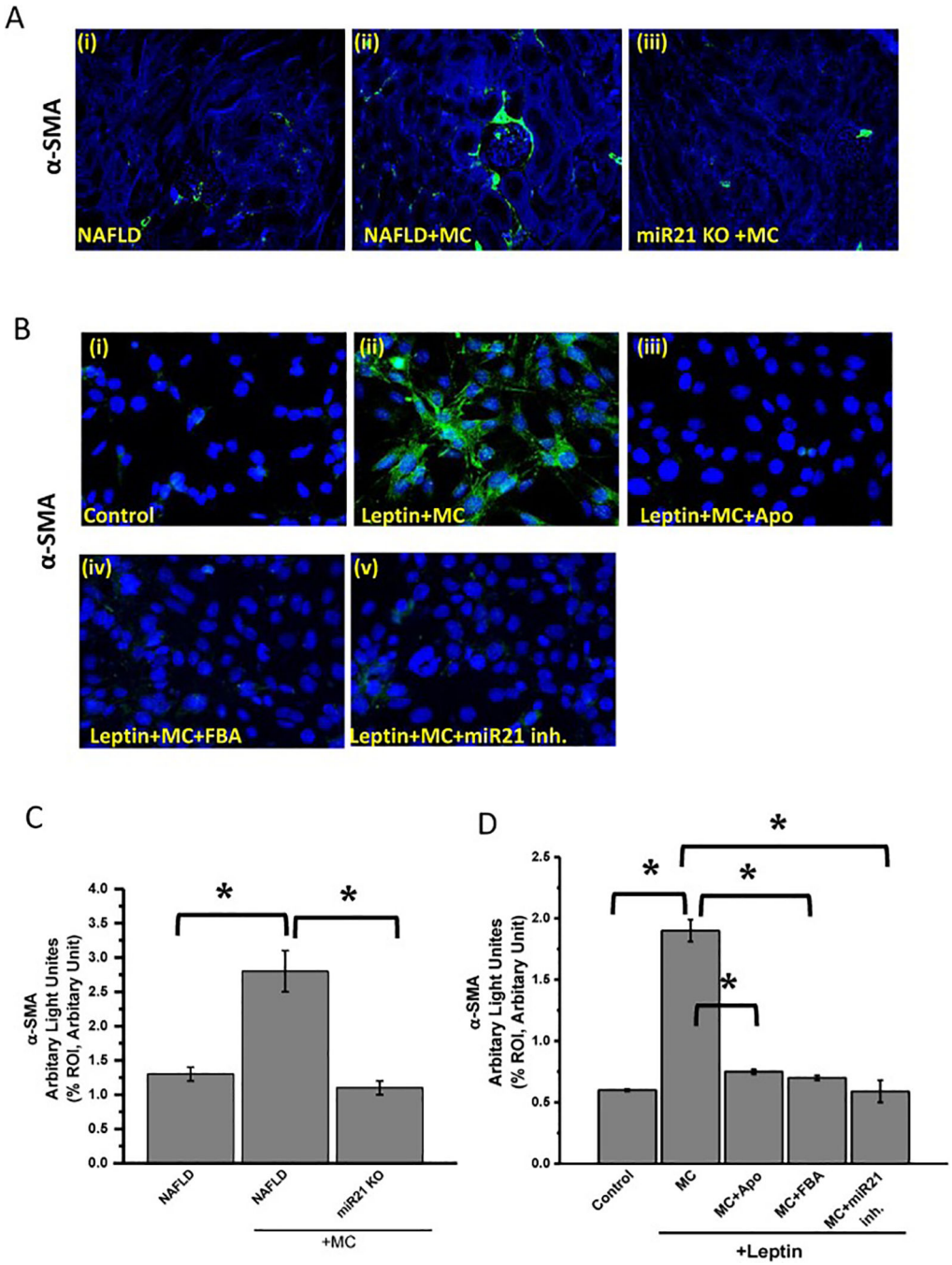

Fig 7:

High expression of miR21 causes mesangial cell activation. **(A) (i-iii)**Formalin-fixed, paraffin-embedded 5 μm kidney tissue sections were used for immunofluorescence staining. Representative α-SMA images as shown by immunofluorescence in kidney slices from NAFLD mice served as a control, NAFLD mice treated with microcystin-LR (NAFLD +MC), and miRNA-21 mice fed with MCD-HFD diet and exposed to microcystin (miR21 KO+MC). Images were taken at 20X magnification. **(B) (i-v)**Immunoreactivity of α-SMA as shown by immunofluorescence images in mesangial cells (control), mesangial cells exposed

to both leptin and microcystin-LR (Leptin+MC), and cells treated leptin and microcystin-LR plus apocynin (leptin+MC+Apo), FBA (leptin+MC+ FBA), or miR21 inhibitor (leptin+MC +miR21 inh.), Images were taken at 40X magnification. **(C)** Morphometric analysis of α-SMA immunoreactivity (mean data from three separate microscopic fields were plotted on Y-axis) in NAFLD, NAFLD+MC and miR21 KO groups of mice. The graph shows a summary of the data, represented as mean SD (n 5 mice per group). Variables were compared for significance using two-way analysis of variance and the Bonferroni test (*,P value between 0.01 and 0.001). **(D)** Morphometric analysis of α- SMA immunoreactivity (mean data from three separate microscopic fields were plotted on Y-axis) in cell control, leptin+MC, leptin+MC+Apo, leptin+MC+FBA, and leptin+MC+miR21 inh. (*P < 0.05). Variables were compared for significance using two-way analysis of variance and the Bonferroni test (*, P value between 0.01 and 0.001).

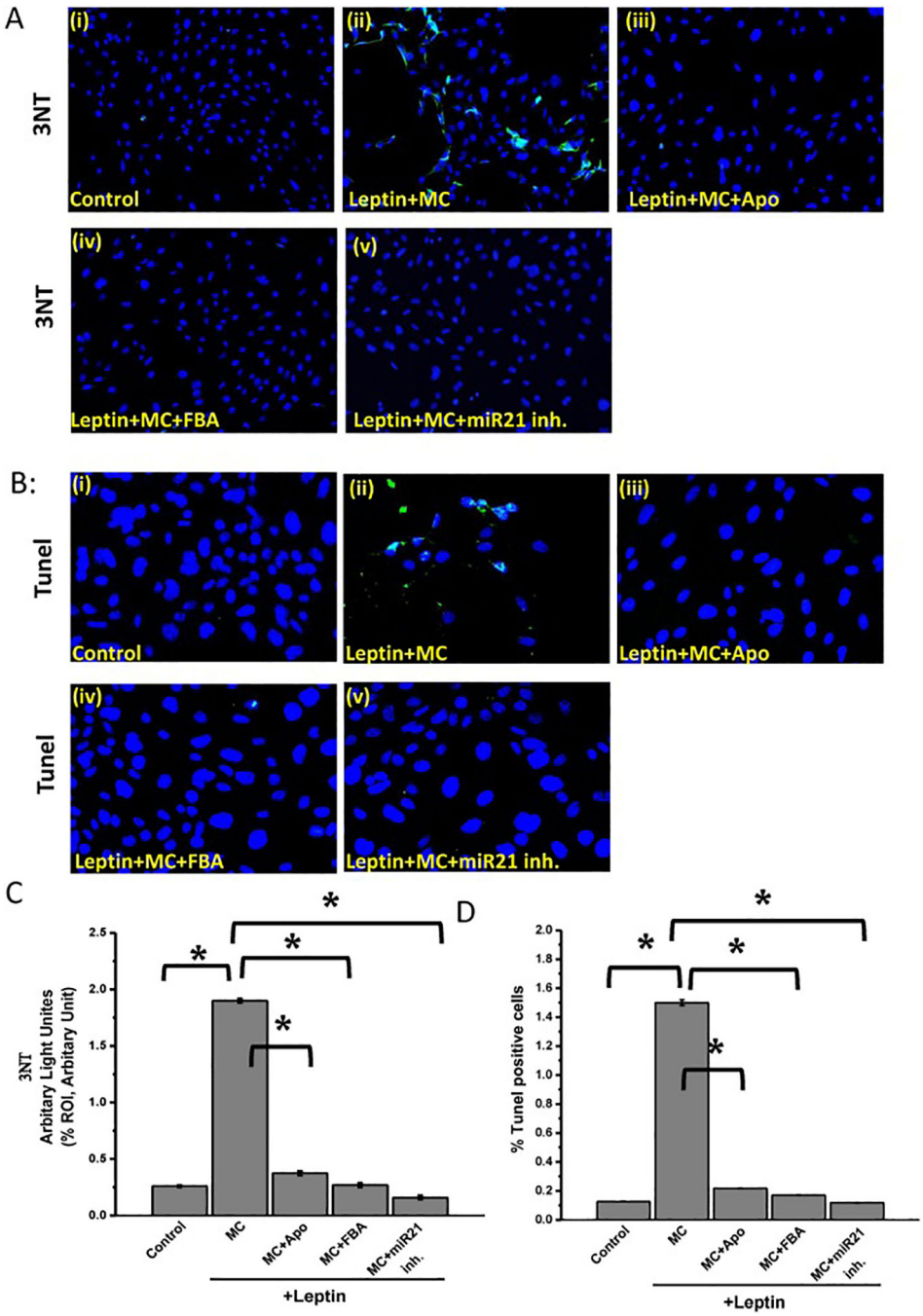

Fig 8: Peroxynitrite- miR21 axis drives mesangial cell activation and cell death:

Microcystin-induced NOX2 generatesperoxynitrite and mir21 activation leads to increased mesangial cell activation and death. Formalin-fixed, paraffin-embedded 5 μm kidney tissue sections were used for immunofluorescence staining. **(A) (i-v)**Immunoreactivity of 3-Nitrotyrosine as shown by immunofluorescence in mesangial cells (control), mesangial cells exposed to both leptin and microcystin-LR (Leptin+MC), and cells treated leptin and microcystin-LR plus apocynin (leptin+MC+Apo), FBA (leptin+MC+ FBA), or miR21 inhibitor (leptin+MC+miR21 inh.). Images were taken at 20X magnification. **(B)(i-v)**

Number of apoptotic nuclei as shown by TUNEL immunofluorescence staining in cell control, leptin+MC, leptin+MC+Apo, leptin+MC+FBA, and leptin+MC+miR21 inh. The number of TUNEL-positive cells identified by their green-stained images were taken at 40X. **(C)** Morphometric analysis of 3NT immunoreactivity (mean data from three separate microscopic fields were plotted on Y-axis0 in cell control, leptin+MC, leptin+MC+Apo, leptin+MC+FBA, and leptin+MC+miR21 inh. (*P < 0.05). Variables were compared for significance using two-way analysis of variance and the Bonferroni test (*, P value between 0.01 and 0.001). **(D)** Percentage of TUNEL-positive cells (obtained by morphometric analysis done on images from three separate microscopic fields) in cell control, leptin+MC, leptin+MC+Apo, leptin+MC+FBA, and leptin+MC+miR21 inh. (*P < 0.05). Variables were compared for significance using two-way analysis of variance and the Bonferroni test (*, P value between 0.01 and 0.001).

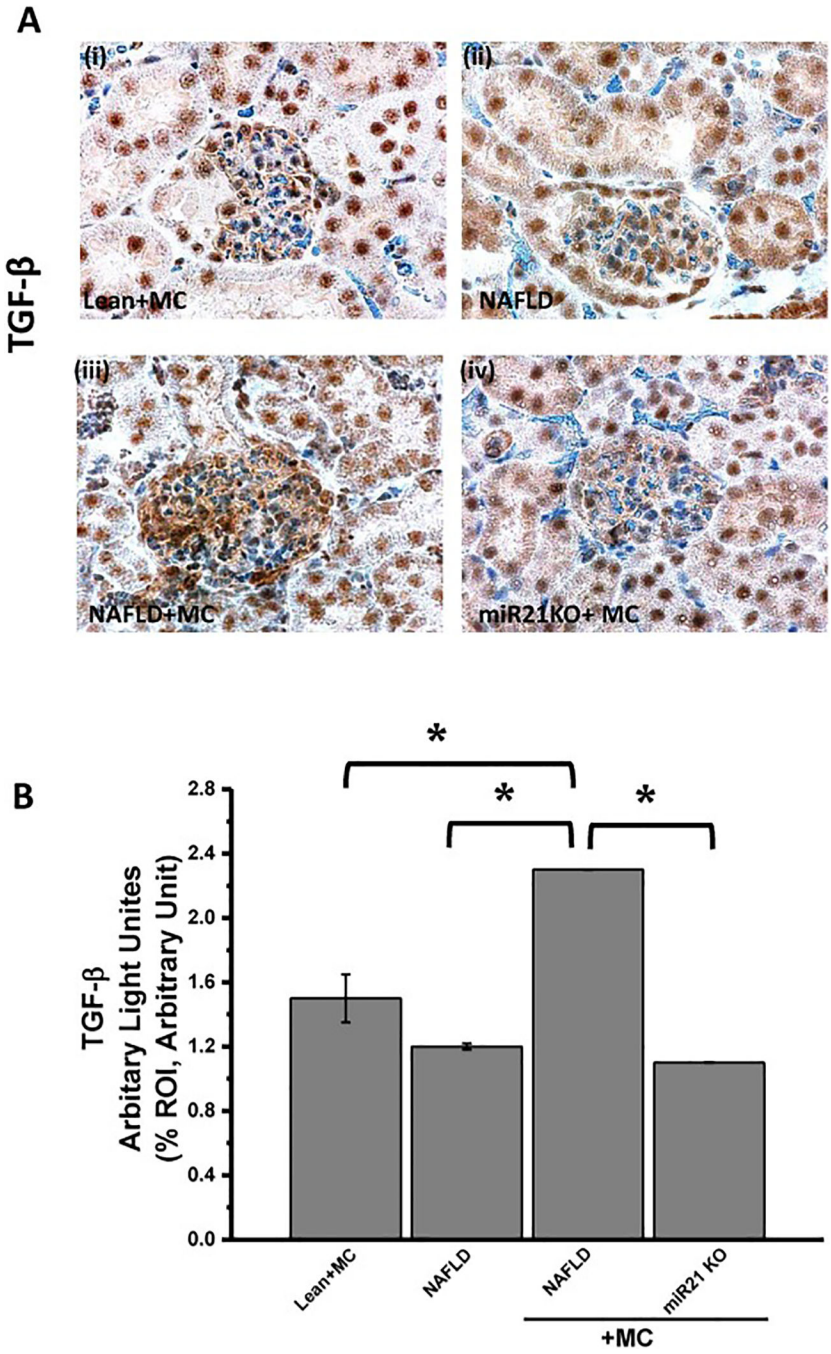

Fig 9: miR21 enhances mesangial cell toxicity via increasing TGF-β.

Formalin-fixed, paraffin-embedded 5 μm kidney tissue sections were used for immunehistochemical technique.**(A) (i-iv)**Immunoreactivity of transforming growth factor (TGF)-β, as shown by immunohistochemistry in kidney slices from lean+MC (i), NAFLD (ii), NAFLD+MC (iii) and miR21 KO + MC (iv) groups of mice. All images were taken at 60X magnification. **(B)** Morphometric analysis of TGF- β immunoreactivity (obtained by morphometric analysis done on images from three separate microscopic fields) in the lean +MC, NAFLD, NAFLD+MC and miR21 KO + MC groups(*$P < 0.05$). The graph shows a

summary of the data, represented as mean SD (n=5 mice per group). Variables were compared for significance using two-way analysis of variance and the Bonferroni test (*, P value Variables were compared for significance using two-way analysis of variance and the Bonferroni test (*, P value between 0.01 and 0.001).

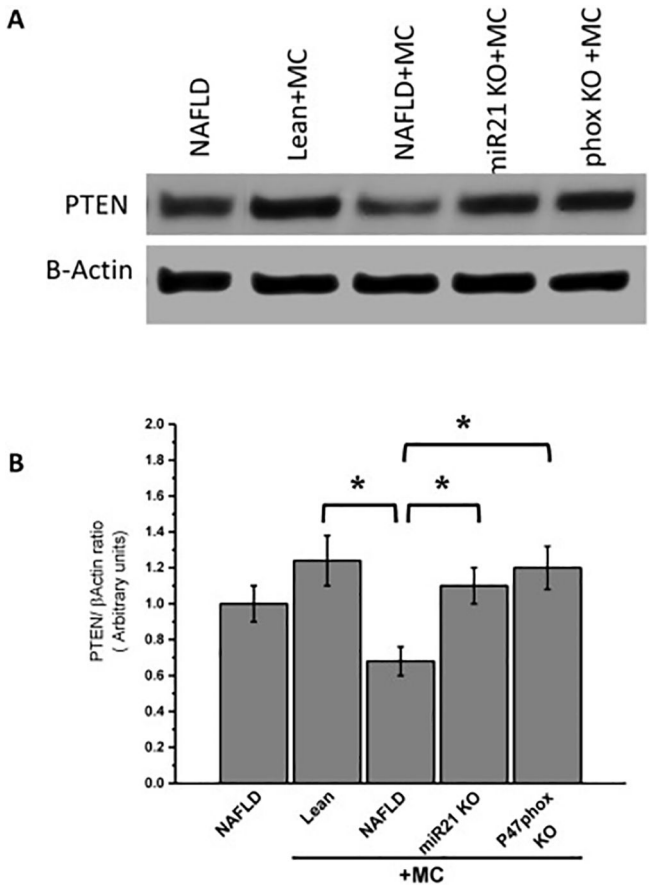

Fig 10. NOX2- miR21 axis causes decrease in PTEN expression in NAFLD kidney following microcystin exposure.

(A) Western blot analysis of PTEN protein levels followed by normalizations against β-actin in lean+MC, NAFLD, NAFLD+MC, and miR21 KO + MC, and P47phox+MC groups. **(B)** Morphometric analysis of PTEN/ β-Actin ratio. Variables were compared for significance using two-way analysis of variance and the Bonferroni test (*, P value between 0.01 and 0.001).

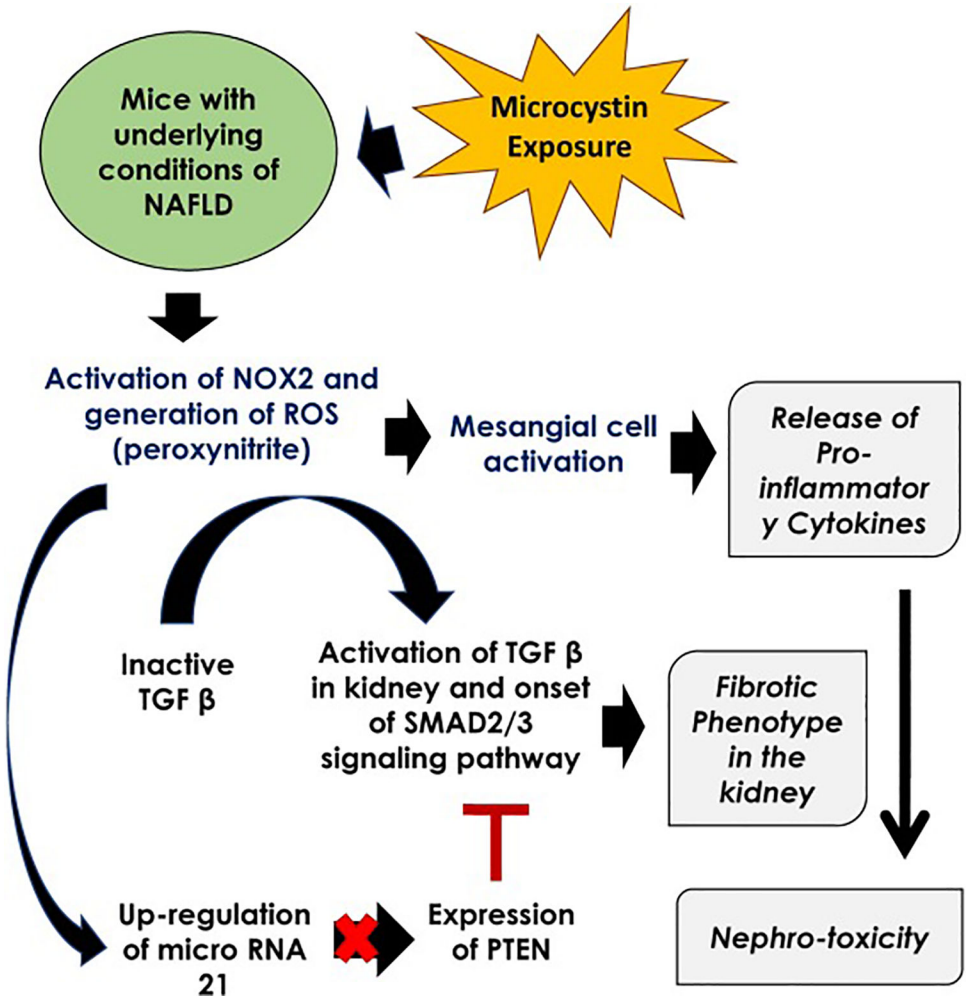

Fig 11.

Pathway Diagram illustrating the mechanism of microcystin toxicity in kidney under the conditions of non-alcoholic fatty liver disease.

Table

showing the primer sequences for the different targets genes:

Target	Species	Sequence 5′–3′
MCP-1 F	*Mus musculus*	GTAGCAGCAGGTGAGTGGGGC
MCP-1 R	*Mus musculus*	CACAGTTGCCGGCTGGAGCAT
IL-1β F	*Mus musculus*	CCTCGGCCAAGACAGGTCGC
IL-1β R	*Mus musculus*	TGCCCATCAGAGGCAAGGAGGA
18SF	*Mus musculus*	TTCGAACGTCTGCCCTATCAA
18SR	*Mus musculus*	ATGGTAGGCACGGCGATA
CD68F	*Mus musculus*	AGGGTGGAAGAAAGGTAAAGC
CD68R	*Mus musculus*	AGAGCAGGTCAAGGTGAACAG
F4/80F	*Mus musculus*	TTTCCTCGCCTGCTTCTTC
F4/80R	*Mus musculus*	CCCCGTCTCTGTATTCAACC